Characterization of a phenol-based model for denervation of the abdominal aorta and its implications for aortic remodeling

Calvin Chao, MD,[a] Caitlyn Dang, BS,[a] Nidhi Reddy, BA,[a] Sara Alharbi, MS,[a] Jimmy Doan,[b] Akashraj Karthikeyan,[b] Brandon Applewhite, PhD,[b] and Bin Jiang, PhD,[a,b] Chicago and Evanston, IL

ABSTRACT

Objective: Sympathetic innervation plays a pivotal role in regulating cardiovascular health, and its dysregulation is implicated in a wide spectrum of cardiovascular diseases. This study seeks to evaluate the impact of denervation of the abdominal aorta on its morphology and wall homeostasis.

Methods: Male and female Sprague-Dawley rats (N = 12), aged 3 months, underwent midline laparotomy for infrarenal aorta exposure. Chemical denervation was induced via a one-time topical application of 10% phenol (n = 6), whereas sham controls received phosphate-buffered saline (n = 6). Animals were allowed to recover and subsequently were sacrificed after 6 months for analysis encompassing morphology, histology, and immunohistochemistry.

Results: At 6 months post-treatment, abdominal aortas subjected to phenol denervation still exhibited a significant reduction in nerve fiber density compared with sham controls. Denervated aortas demonstrated reduced intima-media thickness, increased elastin fragmentation, decreased expression of vascular smooth muscle proteins (α-SMA and MYH11), and elevated adventitial vascular density. Sex-stratified analyses revealed additional dimorphic responses, particularly in aortic collagen and medial cellular density in female animals.

Conclusions: Single-timepoint phenol-based chemical denervation induces alterations in abdominal aortic morphology and vascular remodeling over a 6-month period. These findings underscore the potential of the sympathetic nervous system as a therapeutic target for aortic pathologies.

Clinical Relevance: Aortic remodeling remains an important consideration in the pathogenesis of aortic disease, including occlusive, aneurysmal, and dissection disease states. The paucity of medical therapies for the treatment of aortic disease has driven considerable interest in elucidating the pathogenesis of these conditions; new therapeutic targets are critically needed. Here, we show significant remodeling after phenol-induced denervation with morphologic, histologic, and immunohistochemical features. Future investigations should integrate sympathetic dysfunction as a potential driver of pathologic aortic wall changes with additional consideration of the sympathetic nervous system as a therapeutic target. (JVS—Vascular Science 2024;5:100202.)

Keywords: Abdominal aorta; Sympathetic nervous system; Vascular remodeling; Vascular smooth muscle cell

Vascular diseases, encompassing a spectrum from aortic pathologies to systemic vascular disorders, remain a leading cause of morbidity and mortality worldwide. Among these, aortic diseases such as occlusive disease or aneurysms pose particularly formidable challenges due to their often initially asymptomatic nature and the limited therapeutic options available. The intricate interplay between neural regulation and vascular homeostasis has been recognized as a critical factor in cardiovascular health.[1,2] Specifically, sympathetic innervation plays a pivotal role in modulating the phenotypic behavior of vascular smooth muscle cells (VSMCs), influencing the structural integrity of blood vessels.[3-7] Despite the growing awareness of the significance of the sympathetic nervous system (SNS) in cardiovascular regulation, there exists a notable gap in our understanding of its precise role in maintaining aortic morphology and homeostasis.

Previous studies have identified SNS signaling as a critical regulator of arterial wall homeostasis with potent effects on inflammation and vascular remodeling.[8] Examination of aneurysmal human aortas have similarly identified upregulation of SNS markers and nerve fibers.[8,9] Such findings suggest the SNS is an important mediator in aortic pathophysiology with additional potential as a therapeutic target. Targeting the SNS, such as renal artery denervation, has gained considerable

attention in the treatment of resistant hypertension with successful clinical translation.[10] Similarly, a recent study with preclinical models have demonstrated targeting the SNS via celiac ganglionectomy can reduce progression of atherosclerosis and enhance plaque stability.[11] Despite these efforts, comprehensive investigations into the effects of denervation on the abdominal aorta are scarce. This remains of particular interest as aortic surgery procedures risk potential disruption of sympathetic innervation with unknown sequelae.[12]

This study seeks to address this gap by investigating the denervation of the abdominal aorta in a rat model. The rationale behind this inquiry is grounded in the premise that sympathetic dysfunction may contribute to the pathogenesis of aortic diseases, including occlusive disease, aneurysms, and related vascular complications. Rather than focus on a specific clinical pathology of the aorta, we seek to shed light on the role of sympathetic innervation in maintaining aortic homeostasis. By employing a phenol-based denervation approach, we aim to elucidate late changes in aortic morphology and vascular remodeling after extended follow-up. Drawing from prior reports that pharmacologic inhibition of catecholamine synthesis normalized MMP-2, elastin integrity, and inflammatory markers in a murine aneurysm model, we hypothesized that chemical ablation of SNS fibers via phenol would confer similar effects albeit in a non-aneurysmal model.[8] Similarly, our prior investigation of decellularized aortic conduits was marked by significant pathologic remodeling, perhaps underpinned by lack of innervation.[13] Understanding these effects is not only crucial for advancing our knowledge of the sympathetic regulation of the abdominal aorta but also holds potential implications for therapeutic interventions in aortic pathologies. The outcomes of this research may pave the way for innovative strategies aimed at modulating sympathetic activity for the prevention or mitigation of aortic-related diseases.

METHODS

Animals. All live animal research was approved by the Institutional Animal Care and Use Committee of Northwestern University, and all animal work was performed within the Center for Comprehensive Medicine at Northwestern University (Evanston, IL and Chicago, IL). Male and female Sprague-Dawley rats (Jackson Laboratories), age 3 months, 250 to 300 g, were obtained and allowed to acclimate within animal housing 72 hours prior to any scheduled procedure. All animals were housed within a controlled environment with a 12-hour light-dark cycle and maintained on standard chow and water preoperatively and postoperatively until scheduled euthanasia for tissue harvest.

ARTICLE HIGHLIGHTS

- **Type of Research:** Basic research in rats
- **Key Findings:** Single timepoint phenol-based denervation induces vascular remodeling of the abdominal aorta at 6 months, including increased elastin fragmentation, reduced medial smooth muscle proteins, and increased microvascular density.
- **Take Home Message:** Denervation of the abdominal aorta results in morphologic changes observed at 6 months, suggesting a potential role of the sympathetic nervous system in aortic morphology and wall homeostasis.

Phenol denervation and sham. Briefly, all animals (N = 12; one-half male) underwent midline laparotomy with exposure of the infrarenal aorta. After skeletonization of the infrarenal aorta with removal of visible perivascular nerves, 10% phenol was topically applied from the lowest renal artery to the iliac bifurcation to one-half of the animals (n = 6; one-half male) with a cotton swab (Fig 1, A). Sham controls (n = 6; one-half male) also underwent skeletonization of the infrarenal aorta and received phosphate-buffered saline in an identical fashion. Rats were observed for postoperative complications and allowed to recover without incident.

Vascular ultrasound. Vascular ultrasound imaging was conducted at 3 and 6 months after phenol denervation to monitor aortic remodeling, using an M7/M7T diagnostic ultrasound system equipped with an L14-6S probe (Mindray Bio-Medical Electronics). Baseline and sham aortas did not undergo duplex ultrasound. Animals were anesthetized through isoflurane inhalation, and the abdominal region surrounding the surgical site was shaved and applied with ultrasound gel. Duplex ultrasound with color Doppler was employed to locate the abdominal aorta and inferior vena cava. Imaging was accomplished with simultaneous utilization of both Doppler and B-mode modalities.

Tissue processing and histology. At 6 months after the operation, animals were euthanized by CO_2 inhalation followed by exsanguination. Rat infrarenal aortas were divided from lowest renal artery to iliac bifurcation into four equal segments, termed segment a through segment d (Fig 1, A). All segments were fixed overnight in 4% formaldehyde solution at room temperature, processed through serial ethanol and xylenes washes, embedded in paraffin, and sectioned at 5 µm. Mounted slides were stained with hematoxylin and eosin (H&E), Masson's trichome, and Verhoeff-Van Gieson stain (EVG) for morphologic evaluation following standard protocols.
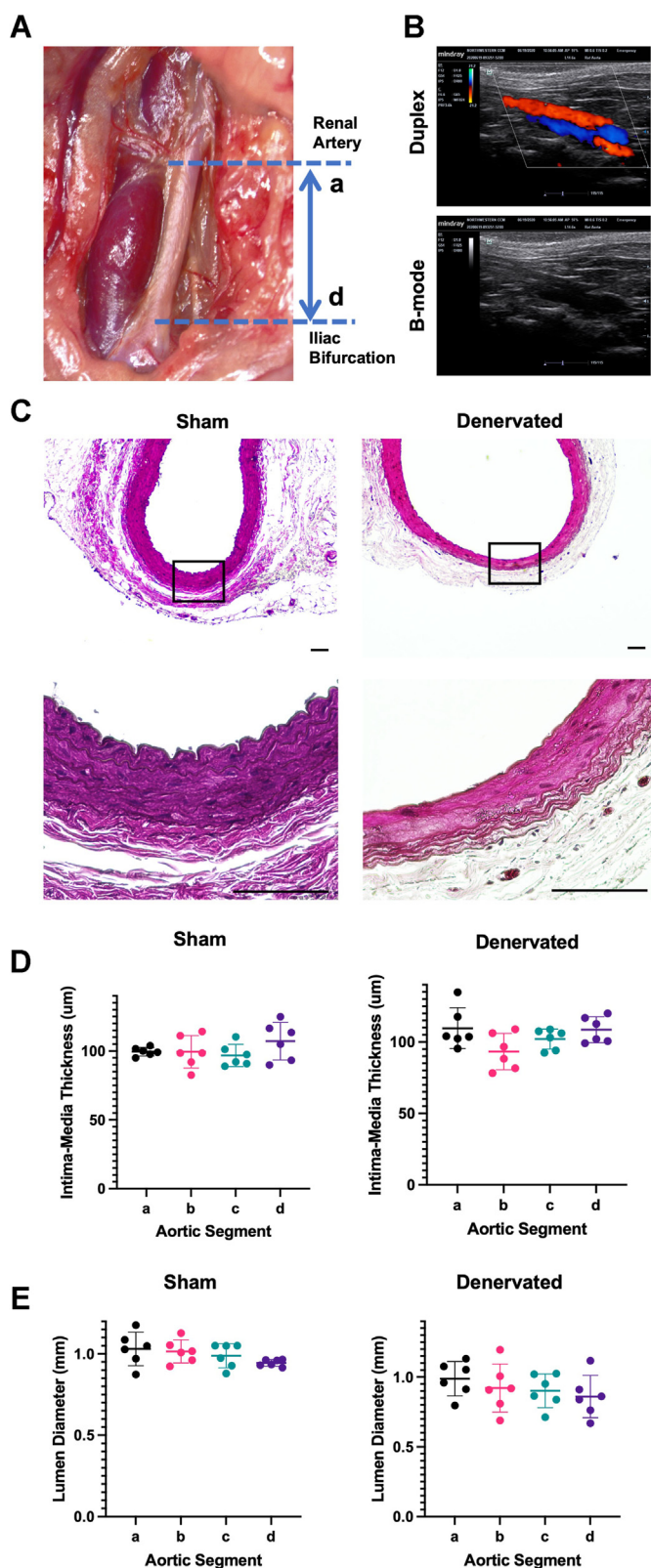
Fig 1. Analysis of aortic wall morphology after phenol-based denervation. **A**, Representative image of surgery indicating the region of the abdominal aorta receiving treatment and the segments for subsequent analysis. **B**, Representative duplex and B-mode ultrasound images of a rat abdominal aorta at 3 months after phenol denervation. **C**, Representative hematoxylin and eosin (H&E) stain of abdominal aortic wall from each experimental group; scale bar = 100 μm. **D–E**, Quantitative analysis of intima-media thickness **(D)** and lumen diameter **(E)** across aortic segments between sham and denervated groups (one-way analysis of variance).

Slides were imaged via brightfield microscopy (Olympus CKX530).

Immunohistochemistry. Samples were treated with ethylenediaminetetraacetic acid (EDTA) for antigen retrieval and incubated with primary antibodies against tyrosine hydroxylase, alpha-smooth muscle actin (α-SMA), myosin-11 (MYH11), runt-related transcription factor 2 (RUNX2), matrix metalloproteinase-2 (MMP2), CD31, and CD68 at 4 °C overnight. After washes, the samples were incubated with fluorescently labeled secondary antibodies and Hoechst dye for 1 hour at room temperature. Images were taken via fluorescence microscopy (EVOS M5000). All antibody information is listed in the Supplementary Table.

Image analysis. Microscopy images were uploaded and analyzed with Fiji.[14] Morphologic measurements, including lumen diameter and intima-media thickness, were conducted utilizing images of H&E-stained sections. Intima-media thickness was measured at eight radially equidistant points per aortic segment by three independent blinded reviewers. Segment b was chosen to standardize subsequent comparisons in aortic morphology. Phenol was applied in a consistent manner from superior (just inferior to lowest renal) to inferior (iliac bifurcation). Segment b avoids potential abutting of the renal ostia while also ensuring adequate phenol application. This segment also demonstrated the lowest intima-media thickness. Elastin breakage scores were determined from four radially equidistant areas per EVG stained aortic segment by three independent blinded reviewers.[15] Collagen analysis was conducted with images of Masson's trichrome stained sections, utilizing color deconvolution and threshold analysis for quantification. Nerve fiber quantification was conducted via immunohistochemical staining of tyrosine hydroxylase, subsequent threshold particle analysis, and normalized to adventitial area. VSMC contractile phenotype was quantified via immunohistochemical staining of medial α-SMA and MYH11. VSMC loss was quantified via immunohistochemical staining of medial α-SMA as well as particle analysis of nuclear count, normalized to medial area. Extracellular matrix (ECM) degradation was quantified via immunohistochemical staining of adventitial MMP2. Angiogenesis was evaluated via immunohistochemical staining of adventitial CD31 and vessel count quantified by three independent blinded reviewers from four radially equidistant images per aortic segment.

Inflammatory infiltration was quantified via immunohistochemical staining of adventitial CD68. Osteogenic changes were analyzed via immunohistochemical staining of medial RUNX2. Four radially equidistant images were taken from each aortic section for all threshold analysis and normalized to medial or adventitial area.

Statistical analysis. Data analysis was conducted using Prism 10.0 (GraphPad Software) and results are presented as means with standard deviation (SD). Morphologic, histologic, and immunohistochemical data were collected from all rats (n = 6 per group), encompassing analyses that combined both sexes and those specific to each sex. The normality of variables was assessed using the Shapiro-Wilk test, and variables demonstrating deviation from normality were evaluated using the Mann-Whitney *U* test. For comparisons across segments a through d, a one-way analysis of variance with Tukey correction for multiple comparisons was employed. To assess differences between the sham and denervated groups, an unpaired two-tailed *t*-test was utilized. A significance threshold of $P < .05$ was considered statistically significant. *P*-values are provided for each data plot with statistical significance. Interobserver variability was assessed via intraclass correlation coefficient for continuous variables and Kendall's coefficient of concordance of ranked categorical variables using R version 3.5.2 with the irr package.[16]

Key reagents. A complete list of key reagents and materials is provided in the supplement (Supplementary Table).

RESULTS

One-time phenol treatment resulted in morphological changes in the aortic walls. All animals successfully tolerated the experimental procedure without any mortality throughout the entire 6-month study period. Vascular ultrasound assessments conducted at 3 and 6 months post-surgery revealed normal blood flow patterns within the denervated abdominal aortas (Fig 1, *B*). The infrarenal abdominal aortas were harvested from all animals at 6 months for detailed histological examination. Transverse cross-sections stained with H&E highlighted noticeable morphological distinctions between the sham and denervated groups, including thinning of the aortic walls after phenol-treatment (Fig 1, *C*). An assessment of the four infrarenal regions (a-d, a = proximal, d = distal) from the denervated group indicated significant variations in intima-media thickness among these regions. Specifically, segment b exhibited the lowest intima-media thickness (93.3 ± 12.7 μm), whereas segment a displayed the greatest intima-media thickness (109.7 ± 14.3 μm; $P = .084$) with an intraclass correlation coefficient of 0.66, indicating good interobserver variability (Fig 1, *D*). In contrast, aortic segments from the sham group showed no significant difference in intima-

media thickness between segments (Fig 1, *D*). Evaluation of lumen diameters demonstrated comparable differences across aortic segments, with gradually decreasing lumen diameter from the proximal to the distal end in both groups (Fig 1, *E*). All subsequent morphologic, histologic, and immunohistochemical analysis was conducted via comparison of segment b between sham and denervated groups.

Phenol denervation altered aortic ECM components. A histologic evaluation of ECM components in the b-segments of aortas from each group was undertaken. Cross sections of aortas from each experimental group indicated similar degrees of collagen content (Fig 2, *A*). Quantification of medial and adventitial collagen indicated no significant difference between denervated (21.4% ± 4.1%) and sham control (17.8% ± 4.6%; $P = .18$) groups. However, when stratifying by sex, denervated females demonstrated significantly increased adventitial and medial collagen content vs sham control (Female: 24.3% ± 2.8% [denervated] vs 15.8% ± 4.2% [sham]; $P = .044$), whereas male animals did not exhibit difference in collagen (male: 18.6% ± 3.1% [denervated] vs 19.7% ± 4.9% [sham]; $P = .74$) (Fig 2, *B*). Additionally, sham aortas demonstrated greater preservation of elastin morphology and reduced elastin fiber breakage in comparison to phenol treated aortas (Fig 2, *C*). Quantification of elastin breakage identified significantly increased elastin breakage scores among phenol-treated aortas (3.0 ± 1.0) vs sham controls (1.2 ± 0.5; $P = .0036$) with a Kendall's coefficient of concordance of 0.79, indicating excellent interobserver variability. Stratification by sex revealed a similar trend (male: 3.1 ± 1.1 [denervated] vs 1.3 ± 0.4 [sham]; $P = .091$; female: 2.8 ± 1.1 [denervated] vs 0.9 ± 0.3 [sham]; $P = .042$) (Fig 2, *D*).

Sexual dimorphism in medial remodeling after phenol denervation. Aortic b segments from each experimental group were evaluated for sympathetic nerve fiber density and vascular remodeling. Sympathetic nerve fibers, indicated by tyrosine hydroxylase positivity, were identified in both sham and denervated groups (Fig 3, *A*). Quantification of sympathetic nerve fiber density revealed a significant decrease after phenol treatment (92.8 ± 20.3 fibers/mm^2) vs sham control (170.4 ± 79.0 fibers/mm^2; $P = .042$). Stratification by sex revealed baseline sympathetic nerve fiber density was much higher in female rats (238.5 ± 39.3 fibers/mm^2) than males (102.3 ± 11.6 fibers/mm^2), and significant denervation was successfully achieved in female animals only (denervated female: 95.4 ± 23.2 fibers/mm^2; $P = .0056$) (Fig 3, *D*).

Alpha smooth muscle actin (α-SMA), a marker of VSMCs, was evaluated in the medial layer of both sham and denervated aortas (Fig 3, *A* and *B*). Quantification of medial α-SMA revealed a significant decrease after phenol treatment (32.6% ± 3.9%) vs sham control
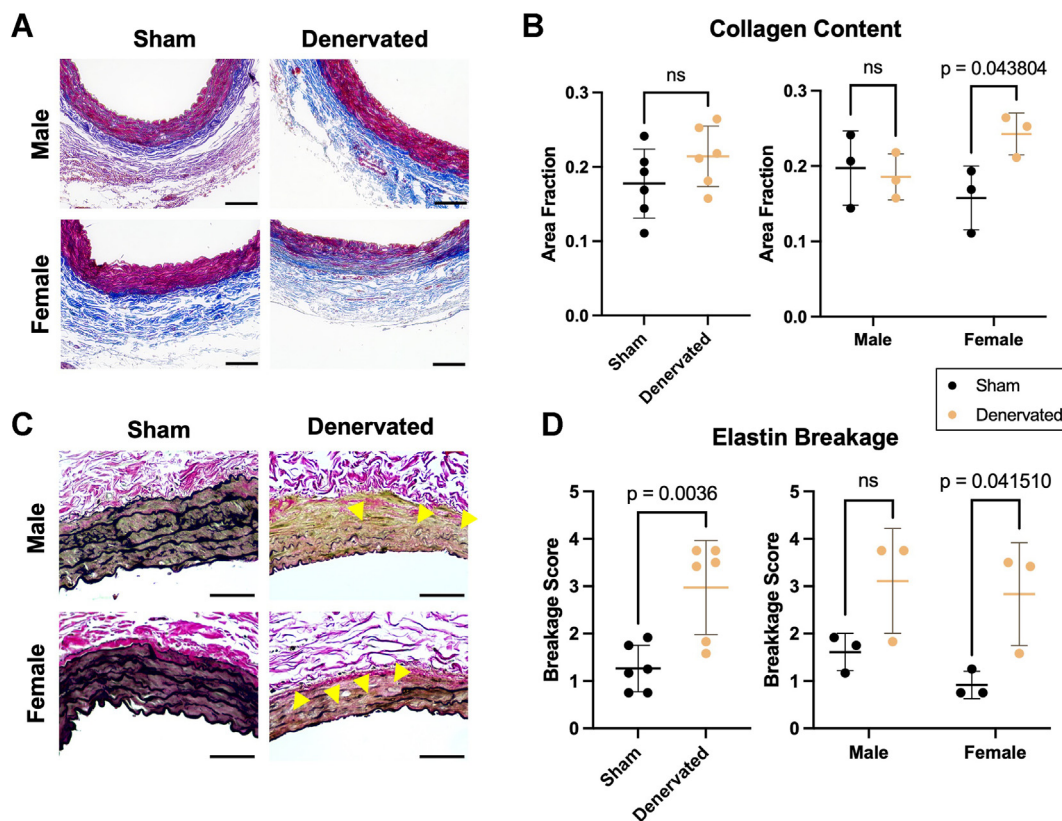
Fig 2. Evaluation of extracellular matrix (ECM) components in response to phenol-based denervation. **A**, Representative Masson's trichrome stain of abdominal aortic wall segment b from each experimental group. **B**, Quantitative analysis of medial and adventitial collagen from sham and denervated groups with and without sex-stratification (unpaired two-tailed *t*-test). **C**, Representative Verhoeff-Van Gieson stain of abdominal aortic wall from each experimental group, with areas of elastin fragmentation indicated by arrows. **D**, Quantitative analysis of elastin breakage score from sham and denervated groups with and without sex-stratification (unpaired two-tailed *t*-test). Scale bar = 100 μm.

(24.6% ± 3.3%; $P = .0034$). Stratification by sex identified this trend was only significant in female animals (male: 26.7% ± 0.8% [denervated] vs 29.5% ± 2.4% [sham]; $P = .12$; female: 22.4% ± 3.7% [denervated] vs 35.6% ± 2.2% [sham]; $P = .0063$) (Fig 3, *E*). MYH11 was similarly evaluated as a marker of contractile VSMCs (Fig 3, *B*). Quantification of medial MYH11 identified a similar significant reduction after phenol treatment (14.2% ± 5.7%) vs sham control (21.6% ± 3.5%; $P = .023$). Stratification by sex revealed similar trends between male and female animals (male: 14.7% ± 7.4% [denervated] vs 22.0% ± 3.0% [sham]; $P = .19$; female: 13.7% ± 5.1% [denervated] vs 21.1% ± 4.6% [sham]; $P = .13$) (Fig 3, *F*).

Potential VSMC phenotypic switch towards osteogenic features was evaluated via immunohistochemical staining of RUNX2 (Fig 3, *C*). No significant differences in medial RUNX2 expression were observed between denervated (0.49% ± 0.44%) and sham (0.65% ± 0.64%; $P = .59$) groups. Stratification by sex identified no significant differential changes in medial RUNX2,

although males demonstrated a negative trend and females a positive trend after denervation (male: 0.13% ± 0.1% [denervated] vs 1.1% ± 0.7% [sham]; $P = .10$; female: 0.85% ± 0.3% [denervated] vs 0.23% ± 0.09% [sham]; $P = .10$) (Fig 3, *G*).

Loss of medial VSMCs was investigated via evaluation of cellular density, indicated by number of nuclei. Quantification of medial cellular density identified a non-significant decrease between denervated (0.0018 ± 0.00025 nuclei/μm^2) and sham (0.0021 ± 0.00038 nuclei/μm^2; $P = .13$) aortas. However, stratification by sex identified a significant decrease in medial cellular density in denervated female animals (male: 0.0018 ± 0.00021 nuclei/μm^2 [denervated] vs 0.0017 ± 0.000095 nuclei/μm^2 [sham]; $P = .71$; female: 0.0017 ± 0.00033 nuclei/μm^2 [denervated] vs 0.0024 ± 0.00011 nuclei/μm^2 [sham]; $P = .03$) (Fig 3, *H*). Notably, no significant changes were detected in medial area between groups (denervated male: 60,355 ± 6684 μm^2 vs sham male: 58,923 ± 12,178 μm^2 vs denervated female:
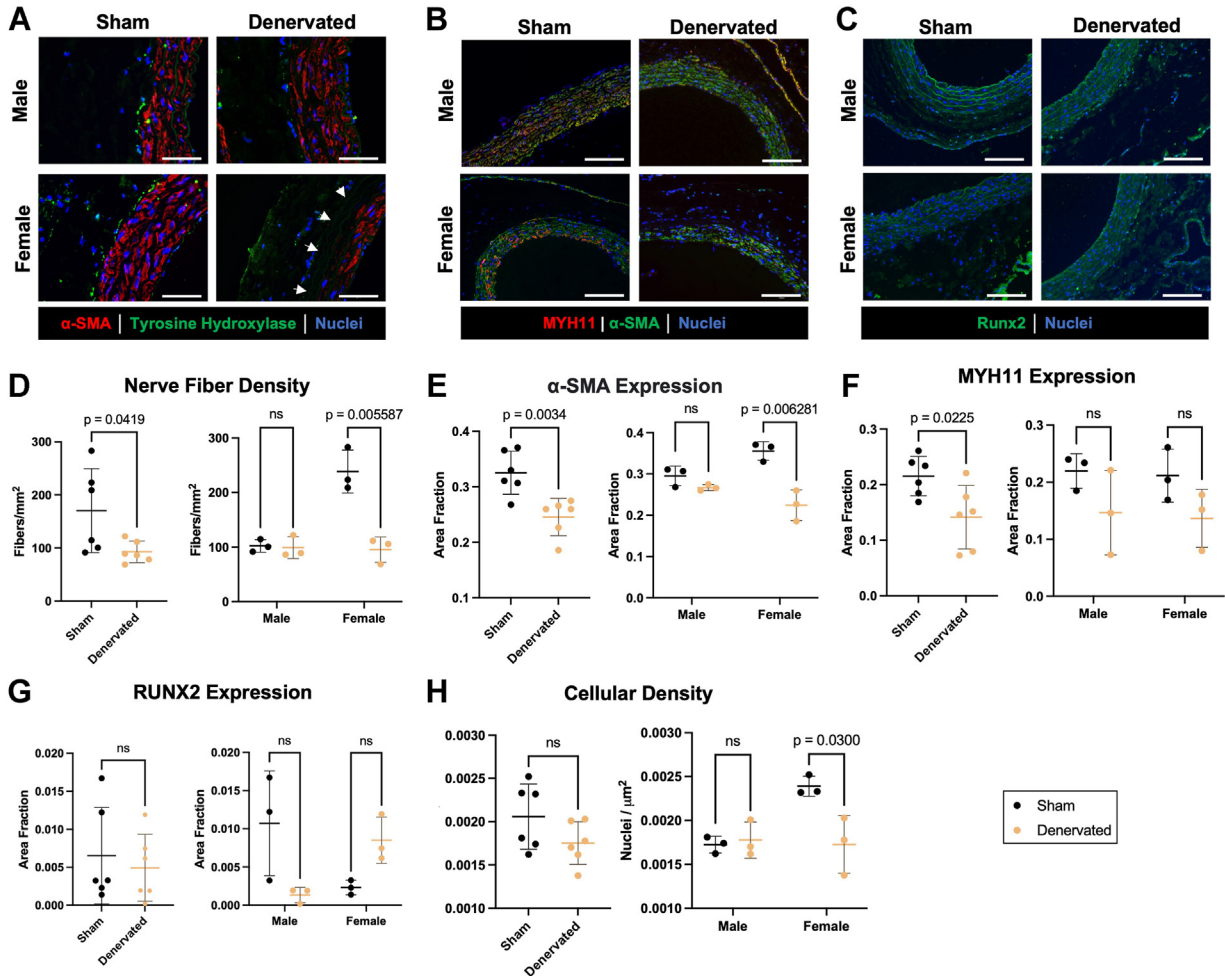
Fig 3. Analysis of vascular remodeling in response to single timepoint phenol denervation. **A,** Representative immunohistochemical staining of α-smooth muscle actin (SMA) (*red*), tyrosine hydroxylase (*green*), and nuclei (*blue*) from each experimental group; scale bar = 75 μm. **B,** Representative immunohistochemical staining of MYH11 (*red*), α-SMA (*green*), and nuclei (*blue*) from each experimental group; scale bar = 150 μm. **C,** Representative immunohistochemical staining of RUNX2 (*green*) and nuclei (*blue*) from each experimental group, scale bar = 150 μm. **D,** Quantification of nerve fiber count normalized against adventitial area from sham and denervated groups with and without sex-stratification (unpaired two-tailed *t*-test). **E,** Quantification of medial α-SMA expression levels from sham and denervated groups with and without sex-stratification (unpaired two-tailed *t*-test). **F,** Quantification of medial MYH11 expression levels from sham and denervated groups with and without sex-stratification (unpaired two-tailed *t*-test). **G,** Quantification of medial RUNX2 expression levels from sham and denervated groups with and without sex-stratification (Mann-Whitney *U* test). **H,** Quantification of medial cellular density from sham and denervated groups with and without sex-stratification (unpaired two-tailed *t*-test).

50,381 ± 817 μm² vs sham female: 53,556 ± 6332 μm²; $P = .40$), indicating these changes reflect alterations in nuclear count. Overall, female animals demonstrated more significant remodeling in the medial VSMCs due to significant changes in sympathetic nerve fiber density after denervation.

Phenol denervation associated with increased angiogenesis in the adventitia. Adventitial angiogenesis, indicated by CD31 positivity, was evaluated between phenol treated and sham aortas (Fig 4, *A*). Quantification of

vascular density via count of CD31 positive vessels identified a significant increase after phenol treatment (60.7 ± 24.1 vessels/mm²) vs sham control (17.2 ± 7.2 vessels/mm²; $P = .0017$). Stratification by sex revealed similar trends between male and female animals (male: 72.8 ± 16.2 vessels/mm² [denervated] vs 14.3 ± 8.2 vessels/mm² [sham]; $P = .012$; female: 48.6 ± 27.4 vessels/mm² [denervated] vs 20.2 ± 5.9 vessels/mm² [sham]; $P = .21$) with an intraclass correlation coefficient of CD31+ vessels of 0.70, indicating good interobserver variability. (Fig 4, *D*). Inflammatory infiltration, indicated by adventitial CD68
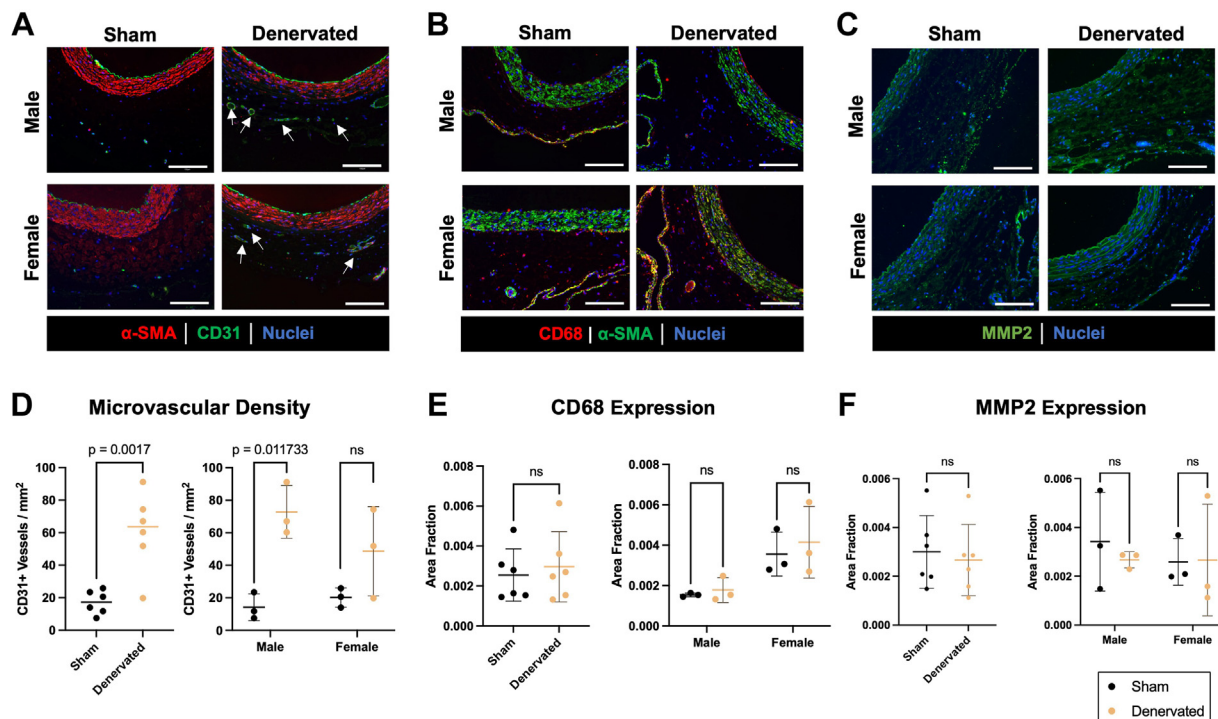
Fig 4. Evaluation of aortic adventitia after phenol-based denervation. **A,** Representative immunohistochemical staining of α-smooth muscle actin (SMA) (*red*), CD31 (*green*), and nuclei (*blue*). **B,** Representative immunohisto-chemical staining of α-SMA (*green*), CD68 (*red*), and Hoechst (*blue*). **C,** Representative immunohistochemical staining of MMP2 (*green*) and Hoechst (*blue*). **D,** Quantification of microvascular density, defined as CD31-positive vessels normalized against adventitial area with and without sex-stratification (unpaired two-tailed *t*-test). **E,** Quantification of inflammatory infiltration, defined as adventitial CD68 area fraction with and without sex-stratification (unpaired two-tailed *t*-test). **F,** Quantification of MMP2 as area fraction of adventitial layer with and without sex-stratification (unpaired two-tailed *t*-test). Scale bar = 150 μm.

positivity, was evaluated between experimental groups (Fig 4, *B*). Quantification of CD68 positivity revealed similar levels between phenol treated (0.30% ± 0.18%) and sham aortas (0.26% ± 0.13%; *P* = .65). Stratification by sex identified comparable responses to denervation (male: 0.18% ± 0.06% [denervated] vs 0.15% ± 0.0092% [sham]; *P* = .54; female: 0.41% ± 0.18% [denervated] vs 0.36% ± 0.11% [sham]; *P* = .65) (Fig 4, *E*). Likewise, no obvious difference in MMP2 expression was observed between sham and denervated groups (Fig 4, *C*). Quantification of adventitial MMP2 area fraction indicated no significant difference after phenol treatment (0.27% ± 0.15%) vs sham control (0.30% ± 0.15%; *P* = .70). Stratification by sex identified similar responses to denervation (male: 0.27% ± 0.033% [denervated] vs 0.34% ± 0.20% [sham]; *P* = .56; female: 0.27% ± 0.23% [denervated] vs 0.26% ± 0.095% [sham]; *P* = .96) (Fig 4, *F*).

DISCUSSION

Maintenance of aortic morphology and wall homeostasis are important considerations in both occlusive and aneurysmal disease states, yet how sympathetic innervation modulates or drives pathology is not well-

elucidated. Here, we demonstrate a novel relationship between sympathetic denervation and vascular remodeling of the infrarenal rat aorta. Notably, our investigation revealed sympathetic denervation induced morphologic and histologic features partially shared with aneurysmal disease, including elastin fragmentation, modulation of VSMC phenotype, loss of VSMCs, and increased angiogenesis.[17] Additionally, sexual dimorphism, which exists in aortic diseases, was also observed in our animal model. Together, our findings further underscore the contribution of SNS-mediated maintenance of the abdominal aorta.

Our model demonstrated denervation of the infrarenal aorta at 6 months after a single timepoint phenol treatment. The selection of phenol for denervation provides multiple advantages in the evaluation of abdominal aortic remodeling. Direct application enables precise delivery to the infrarenal aorta alone and limits the potential for untoward effects of systemic denervation such as in the use of dopaminergic antagonists.[18] Phenol has been extensively employed for topical denervation of diverse arterial beds, including renal arteries and pulmonary arteries, as well as intraparenchymal delivery to solid

organs, including kidney and liver.[19-22] The selection of a rat model not only enhances the technical feasibility of localized denervation but also provides an adequate aortic diameter to serve as a testbed for future investigations of perivascular or intravascular therapies. Our model follow-up of 6 months additionally enables an investigation of vascular remodeling in response to a single timepoint denervation. Pathologies of the infrarenal aorta, including occlusive and aneurysmal disease, demonstrate significant latency prior to manifestation of clinical symptoms. Thus, an extended model enhances the clinical relevance of our study, as our observed findings reflect late vascular remodeling.

The selection of the rat as the experimental model for our study is grounded in several considerations aimed at optimizing the technical feasibility of the model and its relevance to potential future therapeutic applications. The decision to use rats, as opposed to mice, is motivated by the advantageous features of the rat abdominal aorta, including its adequate diameter. This anatomical characteristic facilitates the implementation of surgical procedures and allows for more precise manipulation, contributing to the overall technical feasibility of the model. Furthermore, our prior experience with a rat abdominal aortic interposition model, specifically in the evaluation of decellularized arterial grafts, provided valuable insights. In that study, we observed pathological remodeling and hypothesized that the lack of functional sympathetic reinnervation to the arterial graft contributed to the observed outcomes.[13] This earlier work, coupled with the rationale that the rat abdominal aorta offers a practical and suitable platform for long-term denervation studies, motivated the development of our current model.

Our findings on reduction of α-SMA and MYH11 expression, paired with trends in medial cellular density, reveal the VSMC-specific sequelae of aortic denervation. Other reports have demonstrated VSMC phenotype and survival are dependent on sympathetic innervation.[23,24] Correspondingly, the loss of α-SMA and MYH11 expression likely reflect transition of medial VSMCs away from a differentiated and contractile state. And a reduction in cellular density likely reflects loss of medial VSMCs. Whether this loss reflects upregulation of apoptotic pathways is unclear as catecholamine signaling may potentially also promote apoptosis via suppression of the SMAD-dependent pathway.[24] Phenotypic switch or loss of VSMCs may also contribute to the observed denervation after 6 months. VSMCs are responsible for a number of guidance molecules, including those responsible for arterial innervation such as netrin-1 and ephrin family ligands.[25] Perturbations in VSMC function may thus induce loss of appropriate SNS-VSMC crosstalk, preventing neural regeneration. Phenol denervation induced significant neovascularization of the infrarenal aorta in our model. This is potentially in contrast to

findings from other arterial beds or tumor angiogenesis, in which sympathetic innervation drives neovascularization.[26-28] However, this is perhaps explained by our observations in altered medial VSMC morphology and phenotype. Loss of VSMC contractile features and resultant dedifferentiation towards a synthetic phenotype is critical for both appropriate and pathologic angiogenesis.[29]

Inclusion of male and female animals potentially improves the clinical relevance of our findings as sex differences in aortic disease prevalence are well-documented.[30] Notably, our investigation identified several sex-specific responses to phenol-based denervation. Denervated female animals demonstrated increased aortic collagen content and osteogenic changes but decreased nerve fiber density, actin expression, and medal cellular density. Denervated male animals demonstrated increased vascular density of the vasa vasorum. Although our findings primarily offer descriptive insights, several potential explanations could underlie the observed sex dimorphism. One plausible factor is the influence of sex hormone signaling, which plays a pivotal role in regulating vascular function and remodeling. Additionally, differences in the levels of sympathetic activity between male and female animals may contribute to the observed sex-specific responses to denervation. Future studies exploring the interplay between sex hormones, sympathetic innervation, and vascular remodeling are warranted to further elucidate the underlying mechanisms driving these sex dimorphic responses. Overall, our study highlights the importance of considering sex as a biological variable in investigations of vascular physiology and pathology. By elucidating sex-specific responses to denervation, our findings contribute to a deeper understanding of the complex interplay between sex, sympathetic innervation, and vascular homeostasis.

Our study is not without limitations. Although our model provides anatomic specificity by confining denervation to the infrarenal aorta, surgical exposure introduces a degree of injury to the abdominal aorta, potentially masking subsequent SNS-derived effects. And while the abdominal aorta was exposed in identical fashion between the two groups, the observed effects of phenol denervation could be partially attributed to mechanical damage. Moreover, topical application of phenol may not uniformly denervate the abdominal aorta with predilection for the anterior surface. Our selection of phenol mirrors typical strategies for renal artery denervation, which has demonstrated effects beyond 6 months, comparable to the duration of our model follow-up.[31,32] However, some conflicting studies have reported evidence of renal artery neural regeneration.[33] Thus, although our investigation of nerve fiber density indicates persistent local denervation, the potential for aortic sympathetic neural regeneration is not completely

known. And although the aortic plexus overlying the infrarenal aorta is considered largely sympathetic in nature, denervation of parasympathetic fibers via phenol cannot be fully excluded.[22,34] Whether our observed changes reflect also reflect early phenol-induced changes or subsequent pathologic remodeling is not known. Further early timepoint evaluation and additional investigations of molecular mechanisms after aortic denervation are warranted, as our molecular findings still require validation. Similarly, if abdominal aortic denervation results in systemic effects on other arterial beds, such as the suprarenal aorta, or cardiac tissue, with an impact on systemic blood pressure, is not known but worth investigating for a comprehensive understanding of systemic effects induced by local denervation.

Evaluation of human aortic samples has previously identified increased nerve fiber density corresponding with disease presence.[8,9] And although our investigation has found denervation induces features shared with aneurysmal disease, denervation was applied to otherwise healthy abdominal aortas that likely do not recapitulate the SNS activity in diseased states. Prior investigations of neuroimmune cardiovascular interfaces (NICI) have identified increased regional axonal neogenesis in atherosclerotic aortic aneurysms, with eight- to ten-fold higher tyrosine hydroxylase positive nerves in plaque-burdened segments than plaque-free segments.[11] The same group found celiac ganglionectomy to attenuate progression of atherosclerosis via disintegration of NICIs.[11] However, epidemiological studies have suggested that, although atherosclerosis and AAA may share risk factors, the two may develop in parallel rather than in response to one another.[35,36] Inflammatory pathways may represent a central node that sympathetic innervation acts upon, but potentially lead to opposite downstream effects on atherosclerosis and AAA formation.[37] Ultimately, our findings are limited to an evaluation of healthy abdominal aortic remodeling in response to denervation rather than a direct connection to AAA. Future investigations will need to pair both aortic denervation with pathological models to fully evaluate the role of denervation in aortic pathology.

CONCLUSION

In conclusion, single timepoint denervation induces aortic morphologic changes and aortic wall remodeling. Sympathetic dysfunction is a potent modulator of negative aortic modeling, including elastin fragmentation, loss of contractile features, and aortic neovascularization. Moreover, our model provides a pivotal platform for future investigations of abdominal aortic sympathetic innervation. Our findings underscore the importance of integrating sympathetic innervation in vascular disease states with additional consideration of the SNS as a therapeutic target for cardiovascular disease broadly.

REFERENCES
1. Grassi G, Mark A, Esler M. The sympathetic nervous system alterations in human hypertension. *Circ Res*. 2015;116:976—990.
2. Malpas SC. Sympathetic nervous system overactivity and its role in the development of cardiovascular disease. *Physiol Rev*. 2010;90:513—557.
3. Touyz RM, Alves-Lopes R, Rios FJ, et al. Vascular smooth muscle contraction in hypertension. *Cardiovasc Res*. 2018;114:529—539.
4. Amiya E, Watanabe M, Komuro I. The relationship between vascular function and the autonomic nervous system. *Ann Vasc Dis*. 2014;7:109—119.
5. Jänig W. Sympathetic nervous system and inflammation: a conceptual view. *Auton Neurosci*. 2014;182:4—14.
6. Storkebaum E, Ruiz de Almodovar C, Meens M, et al. Impaired autonomic regulation of resistance arteries in mice with low vascular endothelial growth factor or upon vascular endothelial growth factor trap delivery. *Circulation*. 2010;122:273—281.
7. Pardanaud L, Pibouin-Fragner L, Dubrac A, et al. Sympathetic innervation promotes arterial fate by enhancing endothelial ERK activity. *Circ Res*. 2016;119:607—620.
8. Cañes L, Alonso J, Ballester-Servera C, et al. Targeting tyrosine hydroxylase for abdominal aortic aneurysm: impact on inflammation, oxidative stress, and vascular remodeling. *Hypertension*. 2021;78:681—692.
9. Rodella LF, Rezzani R, Bonomini F, et al. Abdominal aortic aneurysm and histological, clinical, radiological correlation. *Acta Histochem*. 2016;118:256—262.
10. Bhatt DL, Vaduganathan M, Kandzari DE, et al. Long-term outcomes after catheter-based renal artery denervation for resistant hypertension: final follow-up of the randomised SYMPLICITY HTN-3 Trial. *Lancet*. 2022;400:1405—1416.
11. Mohanta SK, Peng L, Li Y, et al. Neuroimmune cardiovascular interfaces control atherosclerosis. *Nature*. 2022;605:152—159.
12. Majd P, Ahmad W, Luebke T, Gawenda M, Brunkwall J. Impairment of erectile function after elective repair of abdominal aortic aneurysm. *Vascular*. 2016;24:37—43.
13. Jiang B, Suen R, Wang JJ, Zhang ZJ, Wertheim JA, Ameer GA. Vascular scaffolds with enhanced antioxidant activity inhibit graft calcification. *Biomaterials*. 2017;144:166—175.

14. Schindelin J, Arganda-Carreras I, Frise E, et al. Fiji: an open-source platform for biological-image analysis. *Nat Methods*. 2012;9: 676—682.

15. Hamblin M, Chang L, Zhang H, Yang K, Zhang J, Chen YE. Vascular smooth muscle cell peroxisome proliferator-activated receptor-γ deletion promotes abdominal aortic aneurysms. *J Vasc Surg*. 2010;52:984—993.

16. Gamer M, Lemon J, Gamer MM, Robinson A, Kendall's W. Package 'irr'. *Various coefficients of interrater reliability and agreement*. 2012;22:1—32.

17. Bruijn LE, van Stroe Gómez CG, Curci JA, et al. A histopathological classification scheme for abdominal aortic aneurysm disease. *JVS-Vasc Sci*. 2021;2:260—273.

18. Haleagrahara N, Siew CJ, Ponnusamy K. Effect of quercetin and desferrioxamine on 6-hydroxydopamine (6-OHDA) induced neurotoxicity in striatum of rats. *J Toxicol Sci*. 2013;38:25—33.

19. Xiao L, Kirabo A, Wu J, et al. Renal denervation prevents immune cell activation and renal inflammation in angiotensin II—induced hypertension. *Circ Res*. 2015;117:547—557.

20. Constantine A, Dimopoulos K. Pulmonary artery denervation for pulmonary arterial hypertension. *Trends Cardiovasc Med*. 2021;31: 252—260.

21. Ye S, Zhong H, Yanamadala V, Campese VM. Renal injury caused by intrarenal injection of phenol increases afferent and efferent renal sympathetic nerve activity. *Am J Hypertens*. 2002;15: 717—724.

22. Hurr C, Simonyan H, Morgan DA, Rahmouni K, Young CN. Liver sympathetic denervation reverses obesity-induced hepatic steatosis. *J Physiol*. 2019;597:4565—4580.

23. Jiao L, Wang MC, Yang YA, et al. Norepinephrine reversibly regulates the proliferation and phenotypic transformation of vascular smooth muscle cells. *Exp Mol Pathol*. 2008;85:196—200.

24. Hu Z, Li B, Wang Z, et al. The sympathetic transmitter norepinephrine inhibits VSMC proliferation induced by TGFβ by suppressing the expression of the TGFβ receptor ALK5 in aorta remodeling. *Mol Med Rep*. 2020;22:387—397.

25. Finney AC, Orr AW. Guidance molecules in vascular smooth muscle. *Front Physiol*. 2018;9:1311.

26. Cen Y, Liu J, Qin Y, et al. Denervation in femoral artery-ligated hindlimbs diminishes ischemic recovery primarily via impaired arteriogenesis. *PLoS One*. 2016;11:e0154941.

27. Zukowska-Grojec Z, Karwatowska-Prokopczuk E, Rose W, et al. Neuropeptide Y: a novel angiogenic factor from the sympathetic nerves and endothelium. *Circ Res*. 1998;83:187—195.

28. Hondermarck H, Jobling P. The sympathetic nervous system drives tumor angiogenesis. *Trends Cancer*. 2018;4:93—94.

29. Ashraf JV, Al Haj Zen A. Role of vascular smooth muscle cell phenotype switching in arteriogenesis. *Int J Mol Sci*. 2021;22:10585.

30. Makrygiannis G, Courtois A, Drion P, Defraigne JO, Kuivaniemi H, Sakalihasan N. Sex differences in abdominal aortic aneurysm: the role of sex hormones. *Ann Vasc Surg*. 2014;28:1946—1958.

31. Eriguchi M, Tsuruya K. Renal sympathetic denervation in rats. *Kidney Research: Experimental Protocols*. 2016;1397:45—52.

32. Rafiq K, Noma T, Fujisawa Y, et al. Renal sympathetic denervation suppresses de novo podocyte injury and albuminuria in rats with aortic regurgitation. *Circulation*. 2012;125:1402—1413.

33. Mulder J, Hökfelt T, Knuepfer MM, Kopp UC. Renal sensory and sympathetic nerves reinnervate the kidney in a similar time-dependent fashion after renal denervation in rats. *Am J Physiol Regul Integr Comp Physiol*. 2013;304:R675—R682.

34. Beveridge TS, Johnson M, Power A, Power NE, Allman BL. Anatomy of the nerves and ganglia of the aortic plexus in males. *J Anat*. 2015;226: 93—103.

35. Johnsen SH, Forsdahl SH, Singh K, Jacobsen BK. Atherosclerosis in abdominal aortic aneurysms: a causal event or a process running in parallel? The Tromsø study. *Arterioscler Thromb Vasc Biol*. 2010;30: 1263—1268.

36. Quintana RA, Taylor WR. Cellular mechanisms of aortic aneurysm formation. *Circ Res*. 2019;124:607—618.

37. Peshkova IO, Schaefer G, Koltsova EK. Atherosclerosis and aortic aneurysm—is inflammation a common denominator? *FEBS J*. 2016;283:1636—1652.